FarmCan: A Physical, Statistical, and Machine Learning Model to Forecast Crop Water Deficit for Farms

Sara Sadri[1], James S. Famiglietti[1], Ming Pan[2], Hylke E. Beck[3], Aaron Berg[4], and Eric F. Wood[†]

[1]University of Saskatchewan, Global Institute for Water Security, SK S7N 3H5, Canada
[2]Scripps Institution of Oceanography, UCSD, La Jolla, CA 92093, U.S.A.
[3]Joint Research Centre of the European Commission, Ispra 21027, Italy
[4]University of Guelph, 50 Stone Road East, Guelph, ON N1G 2W1, Canada
[†]deceased, Nov 2021

Correspondence: Sara Sadri (sara.sadri@usask.ca)

Abstract.

In the coming decades, a changing climate, the loss of high-quality land, the slowing in the annual yield of cereals, and increasing fertilizer use indicate that better agricultural water management strategies are needed. In this study, we designed FarmCan, a novel, robust remote sensing and machine learning (ML) framework to forecast farms' daily crop needed water quantity or Needed Irrigation (NI). We used a diverse set of simulated and observed near-real-time (NRT) remote sensing data coupled with a Random Forest (RF) algorithm and inputs about farm-specific situations to predict the amount and timing of evapotranspiration (ET), potential ET (PET), soil moisture (SM), and root zone soil moisture (RZSM). Our case study of four farms in the Canadian Prairies Ecozone (CPE) shows that 8-day composite precipitation (P) has the highest correlation with changes (Δ) of RZSM and SM. In contrast, 8-day PET and 8-day ET do not offer a strong correlation with 8-day P. Using R^2, RMSE, and KGE indicators, our algorithm could reasonably calculate daily NI up to 14 days in advance. From 2015 to 2020, the R^2 values between predicted and observed 8-day ET and 8-day PET were the highest (80% and 54%, respectively). 8-day NI also had an average R^2 of 68%. The KGE of the 8-day ET and 8-day PET in four study farms showed an average of 0.71 and 0.50, respectively, with an average KGE of 0.62. FarmCan can be used in any region of the world to help stakeholders make decisions during prolonged periods of drought or waterlogged conditions, schedule cropping and fertilization, and address local government policy concerns.

1 Introduction

The Food and Agricultural Organization (FAO) estimates that global food production must increase 50-70% by 2050 to feed the projected population of 10 billion (UN/ISDR, 2007; FAO, 2009). Combined with the increasing frequency of drought due to climate change, non-sustainable use of groundwater, and increasing competition from municipal, environmental, and industrial water needs, farmers are facing the challenge of maximizing crop production without a growing water supply (Han et al., 2018). Farmers across the world, however, may lack adequate means to characterize crop water use, and thus agricultural water management often operates under conditions of unknown water deficiency (Levidowa et al., 2014). Therefore, identifying crop water stress in different growing seasons is necessary to predict yield conditions and plan irrigation scheduling (Virnodkar et al., 2020). Needed Irrigation (NI) or Irrigation Consumptive Water Use (ICU) is the amount of water to reduce crop water stress, satisfy crop water demand, and enhance agricultural Water Use Efficiency (WUE) (Kirda, 2000). In irrigated farms, information on NI can help regulate water deficit, achieve higher levels of crop produced per unit of water consumed, and optimize profit while minimizing potential negative environmental effects (Han et al., 2018; Chalmers et al., 1981; Taghvaeian et al., 2020). However, information on the proper quantity of water to feed crops is also essential in rainfed areas with insufficient rainfall to maintain crop yields and soil conditions (Virnodkar et al., 2020). As climate change and recurring drought continue to impact crop water stress levels and food security, rainfed farms in the U.S. and Canada are increasingly adopting irrigation technologies (USDA-NASS, 2021). For example, the Canadian Ministry of Agriculture is encouraging farmers in Saskatchewan to evaluate their potential NI and apply for irrigation development (Saskatchewan Government, 2022). Knowing the quantity and timings of the water supply gives farmers incentives for more efficient practices such as adopting irrigation, identifying the timing and amount of fertilizers supply, and facilitating more extensive insurance planning and adaptation strategy goals (White et al., 2020; Levidowa et al., 2014; Th.F.Stocker et al., 2013; Geerts and Raes, 2009; Taghvaeian et al., 2020). The timely determination of NI has shown to save water and energy and help farmers achieve improved yields and quality (USDA-NASS, 2021). Several main approaches have been investigated to determine the temporal variability of NI and crop water stress. These methods are based on soil water status, plant responses, and crop modeling using remote sensing data (Taghvaeian et al., 2020; Virnodkar et al., 2020). Most crop water deficit studies have focused on model-based crop water stress, mostly because of the difficulty of measuring water availability for specific agricultural periods such as crop growth or yield (Ash et al., 1992; Wittrock and Ripley, 1999; Quiring, 2004). There have been limited implications for monitoring and predicting farm-specific NI without using in-situ data (Jia et al., 2011). Therefore, providing accurate short-term forecasts of irrigation depth and timing is challenging for soil water balance modeling and other scheduling strategies (Taghvaeian et al., 2020). Smilovic et al. (2016) and Andarzian et al. (2011) employed the crop-water model, Aquacrop, to evaluate the timing and spatial distribution of irrigation water between farms within a watershed in western Canada. They showed that wheat production alone could be maintained while reducing water use by 77%, and production could increase by 27% without increasing irrigation water use. Despite their advantages, NI and crop water stress models can have limited spatial and temporal availability for input data, can be too complicated to operate, and cannot easily be operated as a forecasting tool using remote sensing data. Plant hydraulic models, for example, have relatively complete mechanistic representations of humidity, temperature, and Leaf Area Index (LAI), but they are usually too complex, with many parameters that are hard to measure for crops (Yang et al., 2020).

With Near-Real-Time (NRT) remote sensing, farm NI modeling with reasonable confidence and the potential for better-informed water resources management is now achievable, especially in areas where access or more advanced on-farm technologies are too costly. Remote sensing has been used to calculate vegetation indices (Romero et al., 2018), measure changes in photosynthetic pigment cells (Poblete et al., 2017), measure canopy content and water balance in leaves (Rapaport et al., 2015), and estimate the surface energy balance (Allen et al., 2007). Over the past few decades, Machine Learning (ML) techniques also have been progressively used to process large amounts of information created by remotely sensed data. Several studies have indicated the high significance of addressing plant water stress using ML, which will help farmers improve water and cropland management practices in the low water productivity areas, substantially enhancing the food security (Virnodkar et al., 2020). Various machine learning algorithms, such as Random Forests (RFs), Support Vector Machines (SVMs), Artificial Neural Networks (ANNs), Genetic Algorithms (GAs), and ensemble learning, have been used on remote sensing information in farming (Virnodkar et al., 2020). RF applications have become popular for addressing data overfitting, especially in geospatial classification and prediction of remote sensing data (Vergopolan et al., 2021; Saini and Ghosh, 2018). Poccas et al. (2017) used RF and SVM to model leaf water potential for assessing grapevine water stress. Loggenberg et al. (2018) combined RF with remote sensing data to distinguish stressed and non-stressed Shiraz vines. Despite these advances, scientific NI applications for evaluating crop water stress using remote sensing data have generally remained limited with relatively low adoption by farmers (Virnodkar et al., 2020; Yang et al., 2020; ScienceDaily, 2021). Some of the problems to date are:

1. Lack of access: Many farmers across the globe do not have access to the results of NI models. Therefore, management practices mostly rely on farmers' experience rather than scientific NI models.

2. Lack of timely predictions: Producers need to make NI decisions several days in advance and require tools capable of accurately forecasting short-term crop water use.

3. Complex procedures: Many of these models have tenuous requirements for inputs, time, labor, and financial investment, making the model remain within the scientific domain and out of reach for potential users.

To improve crop water stress and NI deficit management focus should be on: (1) including short-term forecasts in NI schedulers, (2) reducing data, time, labor, and cost requirements for schedulers, (3) providing user-friendly decision support systems, and (4) incorporating remotely sensed data in scheduling (Taghvaeian et al., 2020).

In this study, we developed the FarmCan model to address the abovementioned issues. FarmCan is a hybrid physical-statistical-ML model for NI scheduling and other agricultural applications. At its core, FarmCan is trained on NRT remote sensing data such as surface soil moisture (SM), root zone soil moisture (RZSM), precipitation (P), evapotranspiration (ET), and potential ET (PET) to monitor and forecast daily NI daily and up to 14 days in advance. The contributions of the FarmCan algorithm are to (1) use farm-specific NRT remote sensing data as inputs, (2) use ML to forecast PET, SM, and RZSM using P prediction, and (3) develop a climate-informed forecast of crop NI volume and timing with up to 14 days lead time, (4) allow users to interact with the tool by finding their farms, choosing crop and growing days and getting on a plan that guides and inform them about NI through the growing season, (5) use SM or RZSM depending on the timing and crop growth stage. Our framework is customized for the Canadian Prairies Ecozone (CPE). However, the methodology is generic and can be transferred anywhere to inform farmers and stakeholders where and when additional water is potentially needed to compensate for water deficits. The tool will provide valuable information to governments, agriculturalists, and industries' sustainable initiatives to grow more food and avoid waste with better-managed water, however, ultimately adaptation decisions will need to be made in a more extensive community and government dialogue within management goals.

The remainder of this paper is organized as follows: section 2 describes the study area and the datasets used to train FarmCan; section 3 describes the FarmCan model structure and development; section 4 presents performance and validation of model results. Major conclusions of the study are presented in section 5.

2 Materials and Methods

2.1 Study Area

Over 80% of Canadian farms are concentrated in the CP Ecozone (CPE) (i.e., southern portions of Alberta (AB), Saskatchewan (SK), and Manitoba (MB)) (Wheaton et al., 2005). The CPE has some of the world's highest climate and weather variability. It is predominately continental with long, cold winters, short, hot summers, and relatively low precipitation amounts during the short growing seasons of May to September (Bonsal et al., 1999). The annual mean precipitation is around 478 mm, of which rainfall accounts for almost two-thirds of it during the growing season, and snowfall makes up another 30% of it. Average winter and summer temperatures are -10 °C and 15°C, respectively (Hadwen and Schaan, 2017). Such variabilities significantly affect CPE's agriculture, environment, economy, and culture yearly (Sadri et al., 2020). For example, the drought of 2001–2002 cost approximately $3.6 billion in agricultural production losses (Wheaton et al., 2005). Between 2008 and 2012, federal-provincial disaster relief payouts for climate-related events totaled more than $785 million and more than $16.7 billion in crop insurance. The 100-year record-breaking drought in 2017 caused massive wildfires, reduced yields (particularly canola), heat stress, poor grain fill, livestock feed shortages, and relocation of nearly 3000 cattle in Saskatchewan and Alberta (Cherneski, 2018). The vulnerability of the CPE to agricultural production risks and the future scenarios of climate, which show more severe and frequent droughts with declining precipitation trends and surface water resources during summer and fall, makes the region ideal for developing and testing robust crop NI methodologies.

A total of 4 study farms, on average 160 ha each, were selected within the provinces of SK and MB (Fig1). These farms are sites for other soil moisture core validation networks, such as the Agriculture and Agri-Food Canada (AAFC) RISMA network (Bhuiyan et al., 2018) and the Kenaston Network in Saskatchewan for NASA Soil Moisture Active Passive (SMAP) validation (Sadri et al., 2020; Tetlock et al., 2019). All four farms are rainfed and have alternating crop years (ECCC, 2013). Farmers use pasture, spring wheat, shrubland, and other cover crops to avoid farrow and water-logged conditions in spring. Depending on field and weather conditions, planting typically occurs in late April and early May. For this study, we consider a fixed 7-month window for the growing season: from April 1 to October 31. Table 1 shows that between 2015 to 2019, at least seven different crops were planted on the 4 study farms. Most crops were canola and spring wheat, although there were also soybeans, oats, barley, peas, and lentils. These crops have low to medium sensitivity to drought, and their root depth at maximum growth is anywhere from 0.6 m (lentils and soybeans) to 1.5 m (canola, barley, and spring wheat). The average crop water needs through the growing season are 550 mm; much less was provided by rain as shown in Table 2 (Shuval and Dweik, 2007; Brouwer and Heibloem, 1986). Table 2 shows the amount of precipitation during and outside the growing season. Precipitation outside the growing season is primarily snow. Wind plays a critical role in moving and blowing snow. Therefore, the contribution of melting snow toward meeting future crop water requirements is not substantial and not considered in the FarmCan model. However, establishing soil-water reservoirs or having stubble fields (Pomeroy et al., 1990) can improve snow contribution to SM in the future. Comparing PET with the total annual precipitation, we expect to confirm the amount of water supplied by precipitation is insufficient to meet optimum crop growth.

Table 1. land use from 2015 to 2019.

Study site	**Dominant Land Use [total mm crop water need during growing period]**				
	2015	2016	2017	2018	2019
S1	lentils [325]	canola	barley [450-650]	canola	spring wheat
S2	spring wheat [450-650]	canola	peas [350-500]	spring wheat	canola
M1	canola [450-580]	spring wheat	soybeans	canola	spring wheat
M2	oats [450-650]	soybeans [450-700]	oats	soybeans	oats

*Average crop water use is from FAO guidelines.

Each farm's growing season aridity index (P/PET) is shown in the last column of Table 2. This index is used across the globe to represent vegetation's biogeographical distribution and estimate crop yield (Franz et al., 2020). Based on the aridity index, Manitoba farms have a higher expected crop yield than Saskatchewan farms.

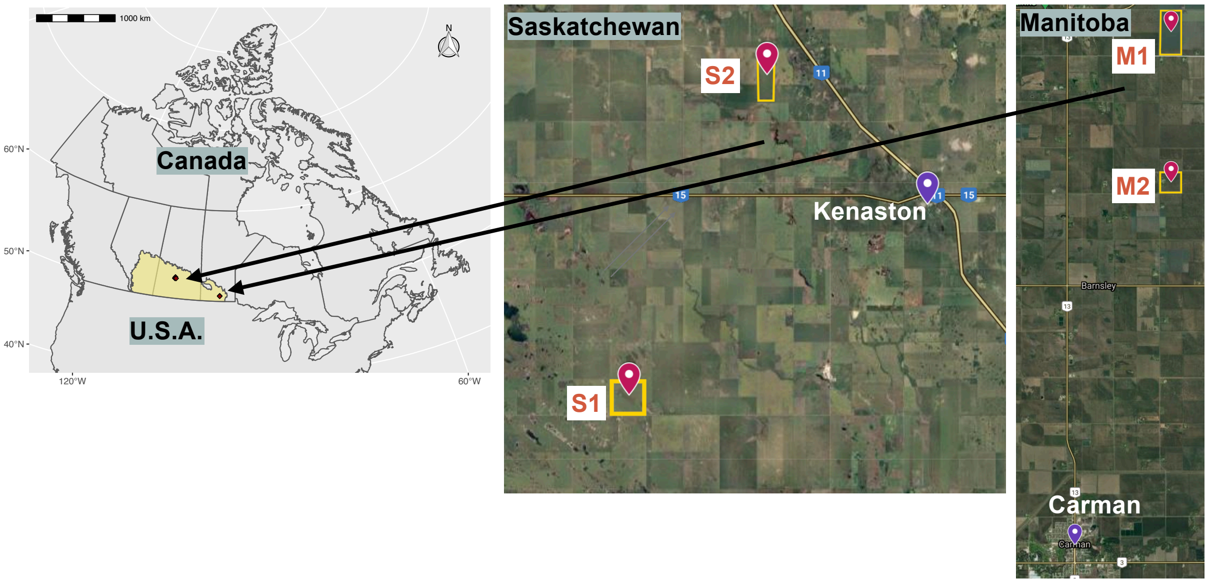

Figure 1. Locations of 4 study farms in Saskatchewan (S1 and S2) near Kenaston, and in Manitoba (M1 and M2) near Carman (©Google Earth 2021).

Table 2. Information about each of the 4 study sites (data from 2015 to 2019).

Study site	Lat	Long	Area [ha]	P[mm] Apr1-Oct31	P[mm] Annual	P/PET [mm/day]
S1	51.42335	-106.46100	263	122.45	146	0.292
S2	51.55185	-106.37318	192	131.62	155	0.282
M1	49.67328	-97.95417	130	167.6	211.7	0.385
M2	49.62460	-97.95435	65	179	221	0.402

* P/PET: aridity index
**PET is the potential ET, obtained from National Atlas of Canada

2.2 Model Components

The two main requirements for the datasets to develop FarmCan are 1) availability of at least five years' worth of NRT remotely sensed data and 2) accessibility of such data in real-time. These two factors would make the FarmCan algorithm trainable and updatable daily. Various datasets were considered, such as Leaf Area

Index (LAI) and the ET from the NASA ECOSTRESS satellite (Fisher et al., 2017), but they did not meet one or both the requirements. On the other hand, MODIS ET and PET products are available and accessible in NRT at 500 meters (m) pixel resolution. The Multi-Source Weighted-Ensemble Precipitation (MSWEP) can provide global P values with a 3-hourly 0.1° resolution covering the period 1979 to the near present (Beck et al., 2019) as an NRT or forecasted product. PET, ET, and P are critical predictors of crop water stress that link the water-energy-carbon cycle (Pendergrass et al., 2020; Brust et al., 2021). SMAP SM products (surface and root zone) are also available and accessible in NRT and provide a highly accurate descriptor of crop stress globally (White et al., 2020). SM is a direct measure of agricultural drought (Sadri et al., 2020; Vergopolan et al., 2021). RZSM becomes important during particular growth stages (mid-season and late-season) and affects crop growth at maturity stage and final crop yield(Smilovic et al., 2019). The inclusion of SM as a dynamic parameter within crop water stress numerical modeling has improved forecast capabilities (Tetlock et al., 2019; Wanders et al., 2014; Koster et al., 2009). The datasets used in this study are listed in table 3.

Table 3. Datasets and the periods used to train and run the model in this study. All input variables were clipped to the CPE domain.

Variable	Dataset	Source	Depth (cm)	Period	Gridded res. (km)	Temporal. res.	Reference
SM	SMAP Level-3 (SPL3SMP)	RS*	5	2015/03/31-2020/12/30	36	Every 3-4 days	(Entekhabi et al., 2014)
RZSM	SMAP Level-4 (SPL4MAU)	Assimilated model	100	2015/03/31 2020/12/30	9	Daily	(Reichle et al., 2019)
P	MSWEP V280	Assimilated in-situ and model	5	1979/01/01-2020/12/30	5	Daily	(Beck et al., 2019)
ET	MODIS	RS	-	2015/01/01-2018/12/30	0.5	Every 8-day**	(Running, 2001)
PET	MODIS	RS	-	2015/01/01-2020/12/30	0.5	Every 8-day**	(Running, 2001)

* RS: Remote Sensing
**8-day composite values

The SMAP satellite was launched in 2015, and the data are available from 31 March 2015 to the present. SMAP Level 3 SM (0-5cm) (SPL3SMP) is a composite based on daily passive radiometer retrievals of global land SM in the top 5 cm of the soil that is resampled to a global, cylindrical ~36 km Equal-Area Scalable Earth Grid, Version 2.0 (EASE-Grid 2.0). For this study, we used version 4 of SPL3SMP retrievals from the morning overpasses to minimize uncertainties and bias from the in-situ data (Al Bitar et al., 2017).

The SMAP Level 4 (SPL4SMAU) is a daily global RZSM product (0-1m) obtained by assimilating low frequency (L-band) microwave brightness temperature observations (for which SPL3SMP is the gridded version) into the GEOS-5 Catchment land Surface Model (CLSM) (Reichle, 2017; Reichle et al., 2015; Sadri et al., 2018), which is driven by surface meteorological data from the NASA Goddard Earth Observation System (GEOS) weather analysis (Brust et al., 2021; Rienecker et al., 2008). Additional corrections using gauge- and satellite-based precipitation estimates downscale to the model's temporal and 9 km scale (Liu et al., 2011) and (Reichle et al., 2011).

ET and PET data are derived from MODIS, a modified MOD16A2/A3 Terra Version 6 (Running, 2001) ET/Latent Heat Flux algorithm. The units are 0.1 kg/m^2/8day (i.e., 0.1 mm/8day), the summation of total daily ET through 8 days (Running et al., 2019). The last acquisition period of each year is a five or 6-day composite period, depending on the year. The algorithm used for the MOD16 data product collection is based on the Penman-Monteith equation, which includes inputs of daily meteorological reanalysis data along with MODIS remotely sensed data products such as vegetation property dynamics, albedo, and land cover. Provided in the MOD16A2 v006 product are layers for composited ET and PET along with a quality control layer from 2001-01-01 to the present. MODIS data are available from 2010 to the present.

MSWEP Version 1 (0.25° spatial resolution) was released in May 2016, and since then has been applied regionally and globally for modeling SM and ET (Beck et al., 2019; Martens and Coauthors, 2017), estimating plant rooting depth (Yang et al., 2016), evaluating root-zone soil moisture patterns (Zohaib et al., 2017), evaluating climatic controls on vegetation (Papagiannopoulou et al., 2017), and analyzing diurnal variations in rainfall (L. Chen and Dirmeyer, 2017), and various other applications (Beck et al., 2019). The product blends gauge-, satellite-, and (re)analysis-based P estimates to improve the accuracy of the estimates globally. MSWEP is a global P product with a 3-hourly 0.1-degree-resolution covering the period 1979 to the present. It does not provide a forecast. However, MSWEP V280 is largely consistent with a newer product, MSWX, that offers medium and longer-term forecasts. Here, we used past dates to build a forecasting tool, so using the MSWEP V280 product was sufficient. For future software development applications, we will use MSWEP combined with MSWX to provide real-time forecasts (Beck et al., 2022).

We used the data in Table 3 in the parsimonious NI model of the FAO

$$NI \approx \sum PET - \sum P - \Delta SM \tag{1}$$

where NI is the volume of water needed to compensate for the deficit between PET as a demand factor, P, and change in soil moisture content (ΔSM or ΔRZSM) as supply factors. All units in equation (1) are in mm. To take care of the unseen delays among system components and reduce errors, we use 8-day composite periods in equation 1 and throughout this study. Eight-day is also consistent with the MODIS output data format.

To convert ΔSM or ΔRZSM volumetric values to depth in equation 1, we multiplied their values by the corresponding depth of the soil (mm) (Allen et al., 1998a, b). For example, a $0.2\mathrm{m}^3/\mathrm{m}^3$ of the surface SM (in the first 50 mm of the topsoil) is equivalent to $0.2 \times 50 = 10\,\mathrm{mm/day}$, whereas the same volumetric soil moisture for the root zone (with a consistent depth of 1000 mm) is equivalent to $0.2 \times 1000 = 200\,\mathrm{mm/day}$, meaning 200 mm of water can be drawn from 1 m deep soil. FarmCan uses 50 mm or 1000 mm depth depending on the crop's development stage. When the crop is in stages 1 or 2, the algorithm uses the first 50 mm depth, and when the crop is in stages 3 or 4, the 1000 mm depth is used.

3 Model Structure

Figure 2 summarizes the design of the main steps for the FarmCan algorithm. The steps include:

1. User inputs the coordinates of a farm, crop type, planting date, and total growing days.

2. The algorithm locates the farm and calculates the dates of each of the four phenological stages of crop growth.

3. From the farm coordinates, the farm center is calculated. Gridded data (i.e., P, SM, RZSM, ET, PET) are clipped from the primary datasets using radii from the farm center calculated in a way that each radius for each variable includes the closest gridded data surrounding the farm perimeter. Calculations of the variables' radii are based on trial and error and the variable's spatial resolution. The farm's specific variable time series is filtered by interpolating the grids outside the perimeter and any of the grids inside the farm. Timeseries data are further processed for the 8-day composite or changed (Δ) values.

4. The variable with the highest correlation with the 8-day P would be the first predictant used to train a Random Forest (RF) algorithm. RF then forecasts that variable for up to two weeks. The predicted

variable would then be fed jointly with the 8-day P as predictors in the next step to predict the next highly correlated variable on the list. The process repeats in a feeding loop and in every round a new variable is first predicted and then used as a predictant.

5. Using equation 1, 8-day NI (NI_{total}) is calculated. If there was no precipitation over the past 8 days, for every antecedent day i, NI_i is $NI_{total}/8$, where $i \in [1,2,...8]$. However, for any amount of P in an antecedent day i, NI_{total} should be adjusted as less supplementary water is needed to compensate for moisture deficit for the days with $P_i > 0$. We calculate daily adjusted weights as:

$$w^i_{adj} = (\frac{800 - \sum_{i=1}^{8} P^i_{deficit}}{8} + P^i_{deficit})/100 \tag{2}$$

where $P^i_{deficit}$ is:

$$P^i_{deficit} = 100 - (100 * (P_i/P_{total})) \tag{3}$$

For example, day i with no precipitation has $P^i_{deficit}$=100% of the P_{total} and a day with 45% of P_{total}, has a $P^i_{deficit}$=55%. The value of 800 is the total deficit percentage in the absence of no rain. Daily distributed amount of NI over 8 days is then calculated as:

$$NI^i_{adj} = w^i_{adj} * NI_i \tag{4}$$

To check the correctness of the calculations above, the relationship $\sum_{i=1}^{8} NI^i_{adj} = NI_{total}$ should hold true.

3.1 Random Forest (RF) algorithm

RF (Breiman, 2001) is an ML method that has shown high accuracy in function estimation and nonparametric regression of geospatial hydroclimatic and space-borne data (Clewley et al., 2017; Vergopolan et al., 2021). The RF algorithm aggregates the predictions made by multiple decision trees of varying subsets called the bagged or bootstrapped datasets. Showing trees different training sets is a way of de-correlating them (Sonth

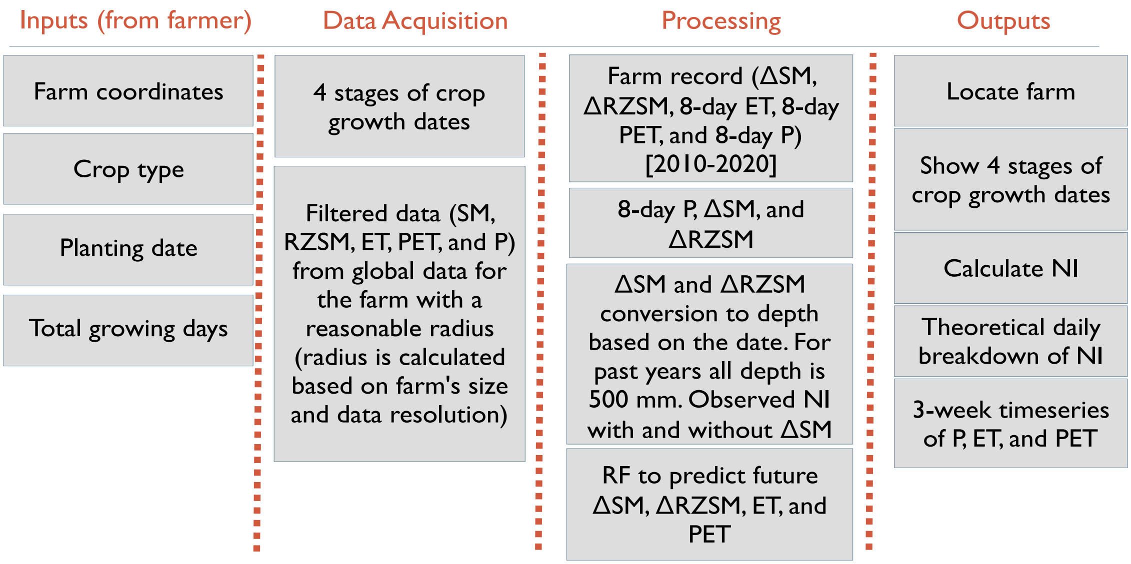

Figure 2. A chart description of the structure of FarmCan.

et al., 2020). It also decreases the variance of the model without increasing the bias, ultimately leading to better model performance. Furthermore, while the predictions of a single tree are highly sensitive to noise in its training set, the average of many trees is not, as long as the trees are not correlated. FarmCan model uses RF in two stages: 1) to fill in the gaps of missing ΔSM and ΔRZSM based on 8-day P from 2010 to 2020 and 2) to predict ΔRZSM, ΔSM, 8-day ET, and 8-day PET up to 14 days in advance. We divided the datasets from 2010 to 2020 into training and testing in a 0.7 to 0.3 ratio.

$$\hat{f} = \frac{1}{B}\sum_{b=1}^{B} f_b(x') \tag{5}$$

The first round of running RF uses 500 decision trees. The optimum number of trees is the one that minimizes the MSE between the training and testing datasets. The second round of running RF involves dictating the optimum number of trees. If a training set $X = x_1, ...x_n$ (n being the number of training samples) has responses $Y = y_1, ...y_n$, the algorithm selects random samples with the replacement of the training set for B times. In equation 5, for $b = 1, ...B$ training samples from X, Y, called X_b, Y_b, produce a regression tree f_b. After training, predictions for unseen samples x' can be made by averaging the predictions from all the individual regression trees.

4 Results

4.1 Spatial comparison of hydrological variables

Figure 3 shows the key variables' 20th, 50th, and 80th percentiles from 2015 to 2020 during the growing season (April to October). Comparing P with the ET and PET map shows that, region-wide, crops do not receive the water needed from rain to reach an optimal yield. Growing season's P is typical of sub-humid and semi-arid climates (Allen et al., 1998a), i.e., the amount of rainfall is often not sufficient to satisfy the water needs of crops. Except for portions of the province of AB, most CPE farming relies on rainfall and, therefore, is vulnerable to agricultural drought (Maybank et al., 1995; McGinn and Shepherd, 2003; White et al., 2020).

Most of Saskatchewan is identified by the lowest amount of SM, P, and ET throughout the growing season. Surface SM is generally lower than RZSM across all three provinces. This is expected as soil at the surface is affected directly by transpiration and wind. In contrast, the soil at the root zone holds onto the water longer, especially as brown-black chernozemic clay, a typical type of soil in the CPE.

4.2 Relative importance of FarmCan inputs

We ran a two-by-two Pearson correlation analysis with a 99% significance level for the four selected farms and during the 7-month growing seasons from 2015 to 2020 (Figure 4).

The four farms' results show that the correlation between P and ΔRZSM and P and ΔSM is quite similar in M1 and M2. However, the correlation between P and ΔRZSM is slightly higher in S1 and considerably higher in S2. Although it is generally expected that instantaneous surface soil moisture shows more variability with P, this study is based on the 8-day cumulative P and changes in 8-day SM, not a direct measure of P

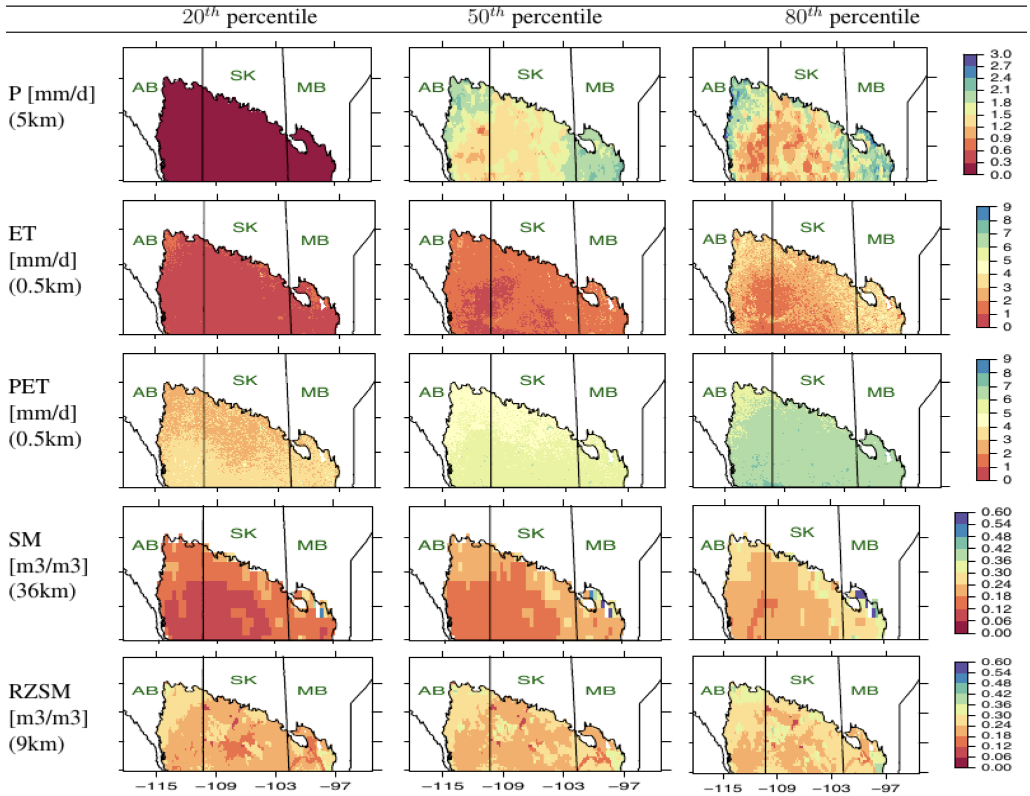

Figure 3. Spatial patterns of variables used for the CPE. Data collected from 2015-2020 for the agricultural months (April-October). AB: Alberta, SK: Saskatchewan, MB: Manitoba.

vs. SM. For example, if the total amount of P over eight days is 20 mm, the RZSM can change from 0.2 to .9 m^3/m^3, which gives a higher ΔRZSM than ΔSM, which might have fluctuated instantaneously but essentially changed from 0.3 to 0.5 over eight days. However, more studies in different regions must confirm such correlations. We speculate that soil type plays a role in how soil maintains moisture at different depths.

There is also no evidence of significant feedback from ET to SM and vice versa. This can be because the relationship between SM and ET, in terms of feedback, mainly depends on the climate (I.Seneviratne et al., 2010). During the growing season, the condition in CPE is either too wet, which makes the total energy for

ET independent of SM, or too dry, which makes ET show little impact on fluxes because it is little or no moisture available.

Generally, a significant impact of SM on ET should be more noticeable in a transitional regime, where soil water supply is available and sufficient (Yang et al., 2020; Running et al., 2019; I.Seneviratne et al., 2010; Famiglietti and Wood, 1994). More studies from different regions are required to understand such interactions in SM and ET fluxes.

All four farms show a significant negative correlation between soil moisture values with 8-day NI within 99% confidence.

4.3 Feedback from a supply-demand mechanism

To study the relationship between water supply and demand in the CPE, we conducted a 3-way comparison of changes in 8-day P supply with variability in ΔSM and ΔRZSM (supply). We also included changes in 8-day ET and 8-day PET (demand factors) in a correlation plot shown in Figure 5. Each row represents a province with the supply variables on the XY axes. For each region, the two left plots show the relationship between 8-day P and ΔSM. Color changes correspond with 8-day PET and 8-day ET. The two right-side plots are the same, except that the Y-axis represents ΔRZSM instead of ΔSM.

Manitoba shows the most robust linear relationship between 8-day P and ΔRZSM. In contrast, Alberta shows the weakest linear relationship between 8-day P and Δ RZSM, likely because most Alberta farms are artificially irrigated. Δ RZSM is more responsive to the amount of 8-day precipitation, meaning that over an 8-day increase of P, RZSM increases. Such a linear relationship is weaker between 8-day P and ΔSM. This can be because surface SM is also affected by exposure to other physiological elements such as wind, elevation, transpiration, and land cover.

There are also visible linear relationships between the 8-day PET and 8-day P, especially in Manitoba and Saskatchewan. The 8-day PET (and less for 8-day ET) tend to increase with higher 8-day P. The 8-day ET and 8-day PET do not show a linear correlation to the ΔSM, although for periods which 10 mm < eight-day P < 40 mm, 8-day PET values tend to have a positive trend when the ΔSM is decreasing (negative). When eight-day P > 40 mm, Saskatchewan and Alberta showed more mid-range PET (20-60 mm/8 day). This can mean SK and AB are regularly in dry conditions when the water supply is less than optimum. MB is generally moist but can range from adequate crop water availability to extreme water stress periods. The atmospheric demand is typically low for periods with 8-day P less than 10 mm. In all plots, the average 8-day PET is higher than the 8-day ET, which shows that a higher-than-supplied atmospheric demand exists throughout the growing season at the CPE.

4.4 Time series of data and calibration period

Figure 6 is the variability plot of farm S2 from 2015 to 2020. Each year's 7-month agricultural period is shown on pink background. A negative ΔSM or ΔRZSM means a decrease in SM or RZSM, respectively, over the eight days intervals and vice versa.

During every agricultural year, the SM reacts to P with much higher variability and sensitivity than ΔRZSM. Although instantaneous rain is more correlated with the SM, as previous results showed, 8-day P shows a higher correlation with Δ RZSM. In the CPE, ΔRZSM generally reverts to zero, indicating a weakly stationary behavior. However, the amount and timing of daily RZSM can still be insufficient to support effective crop growth. As for surface SM, the changes do not seem stationary. The 8-day PET is consistently higher than 8-day ET, confirming that crops receive less than the optimal amount of their water demand throughout the year. We plotted variability plots for the other three farms (not shown here), and the patterns were consistent with those from farm S2.

4.5 FarmCan prediction process

To illustrate the FarmCan real-time forecast process, we describe an example where 2020/07/02 is "today's date", the crop type is barley, the planting date is 2020/04/01, and the whole growing season is 150 days. The FarmCan algorithm uses these inputs and the FAO guidelines to provide the expected dates of stages 1 to 4, as shown in Table 4.

Table 4. Key dates relevant to barley planted on 2020/04/01. From FAO guidelines (Allen et al., 1998a).

Stage	Stage ending date
1: initial	2020/04/15
2: crop development	2020/05/14
3: mid season	2020/07/17
4: late season	2020/08/25

The observed variables are plotted for the assumed date in Figure 7(a). The total period shown in the plot is 21 days, from 2020/06/22 to 2020/07/12. The green bars are the daily precipitation from MSWEP, including the forecast values. The hindcast NI, shown by the grey bars, is distributed by calculating w_{adju}. Because 2020/07/02 corresponds to the 3rd stage of crop development, FarmCan predicts ΔRZSM (instead of ΔSM) and 8-day PET using the RF algorithm. The algorithm then calculates 8-day NI (in mm) for the remaining days shown in Figure 7(b). Note that the information in Figure 7(a) is repeated in Figure 7(b). Figure 8 shows only the predictions for farms S2, M1, and M2.

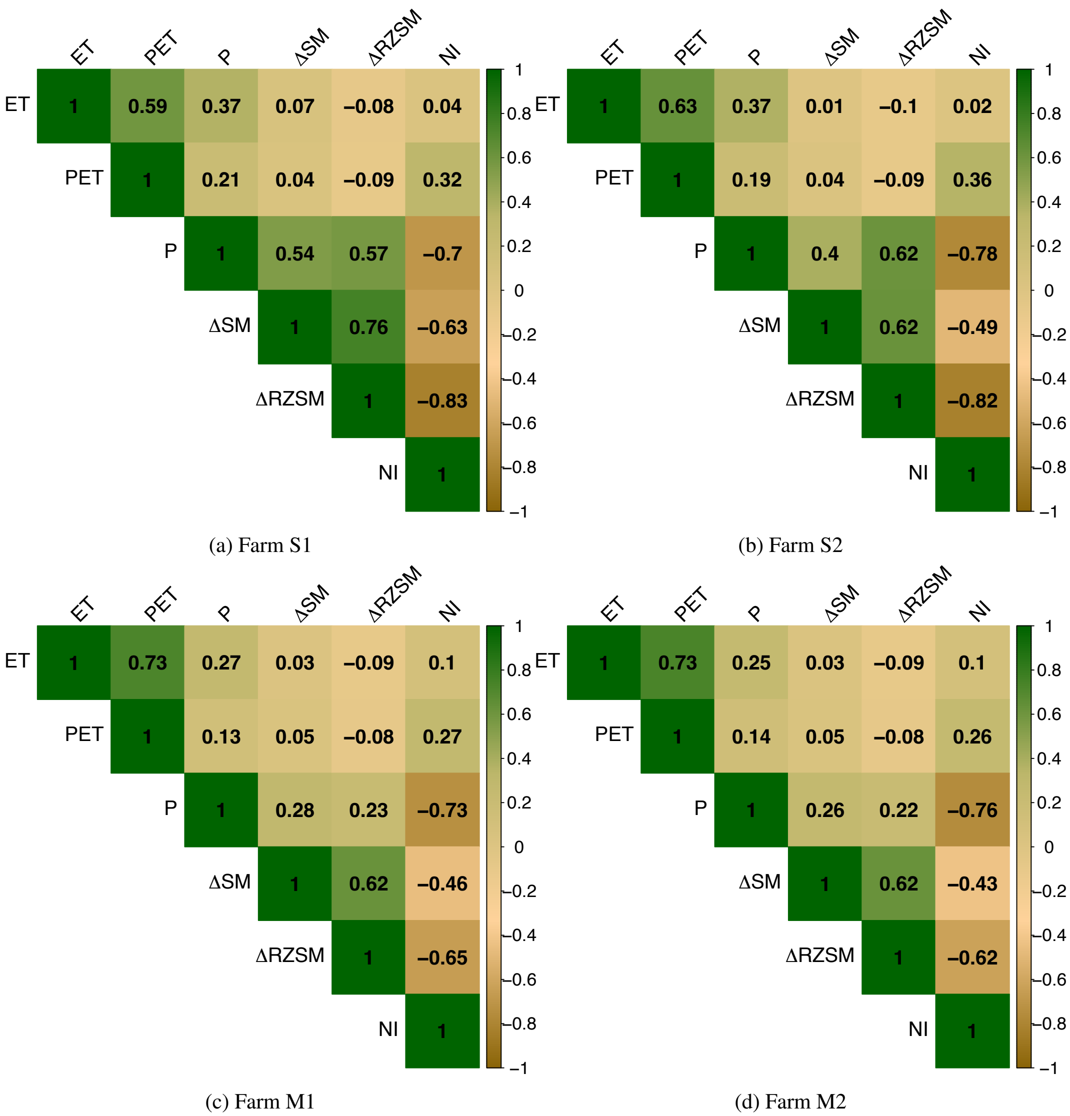

Figure 4. Pearson correlation relationship between observed 8-day ET [mm/8d], PET [mm/8d], P [mm/8day], ΔSM [m^3/m^3], ΔRZSM [m^3/m^3], and NI [mm/8d] for farms S1, S2, M1, and M2 during agricultural years [2015-2020]. Significance level: 99%.

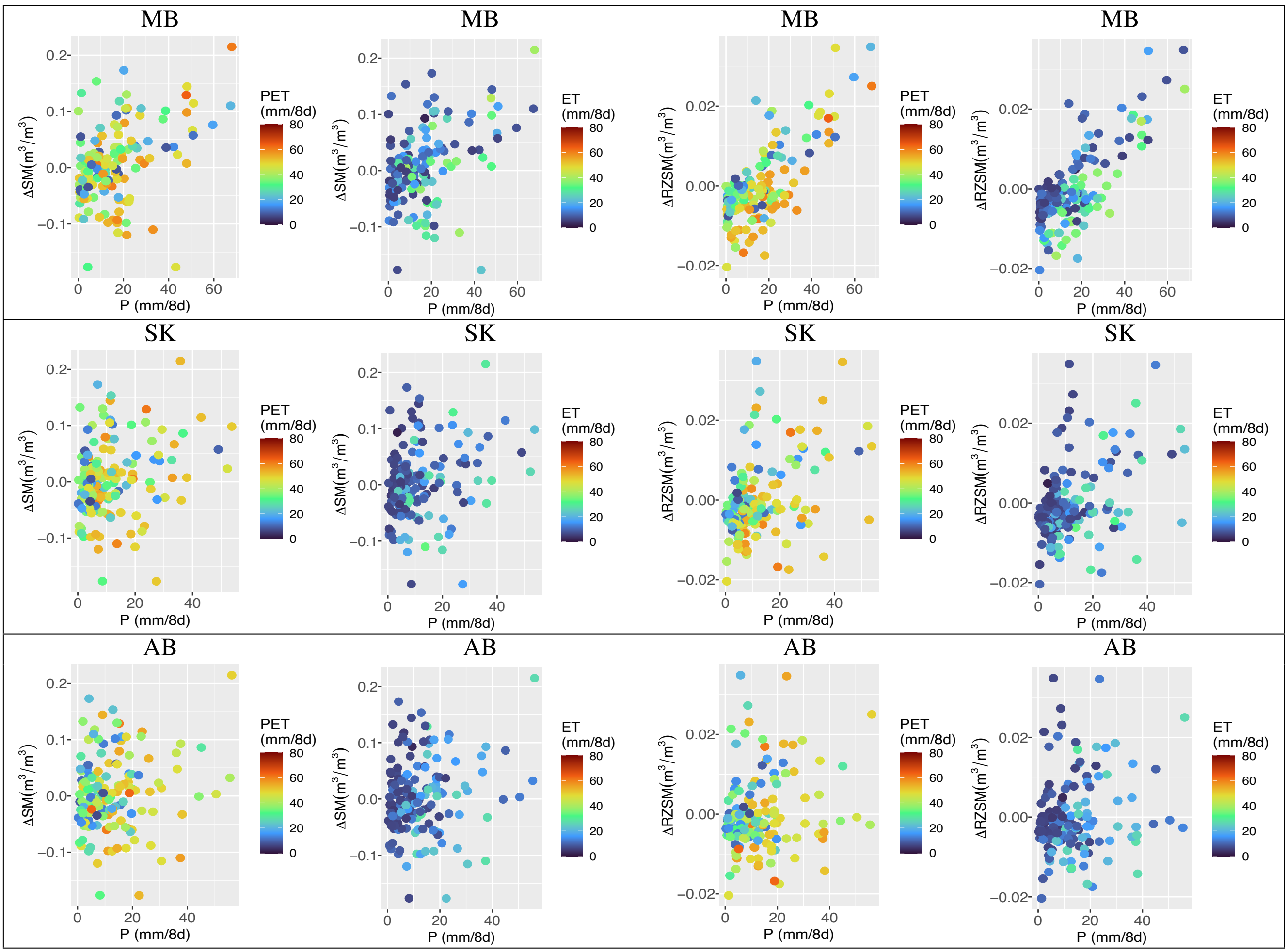

Figure 5. Changes of 8-day P, ΔSM, and ΔRZSM (supply) with 8-day ET and 8-day PET (demand). Each row shows one province. Data was collected from 2015-2020 for the agricultural year (April-October).

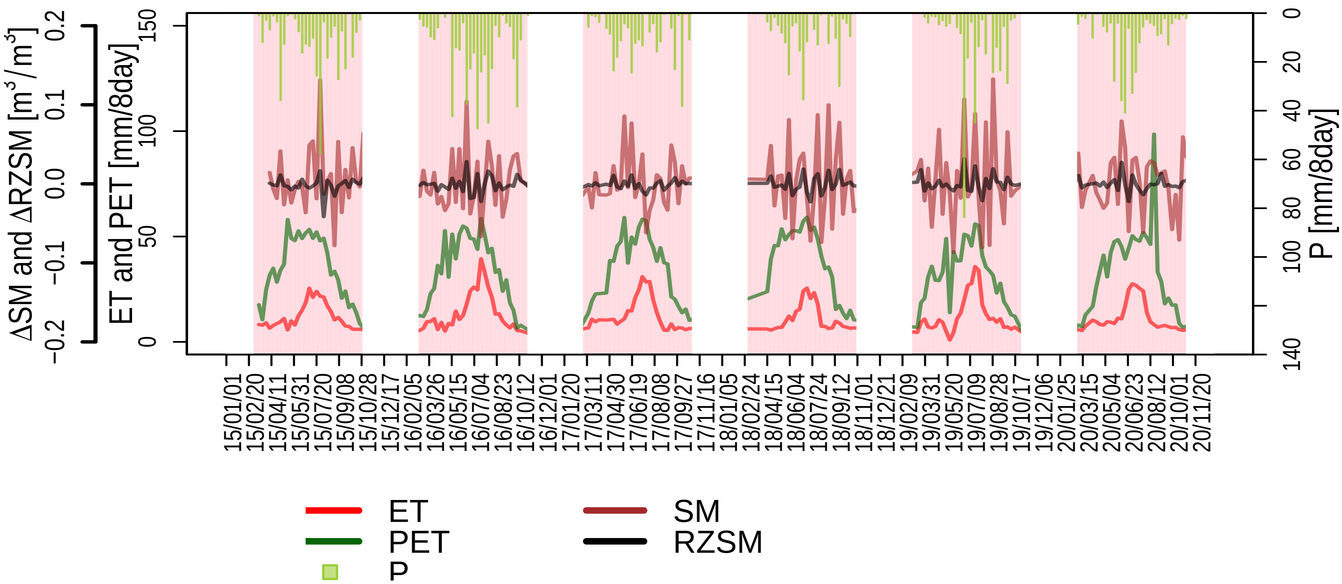

Figure 6. 8-day variability analysis, Farm S2 [2015-2020]. Pink background indicates the agricultural period. Green: PET, Red: ET, Purple: ΔSM, Balck: ΔRZSM, and Teal: 8-day P.

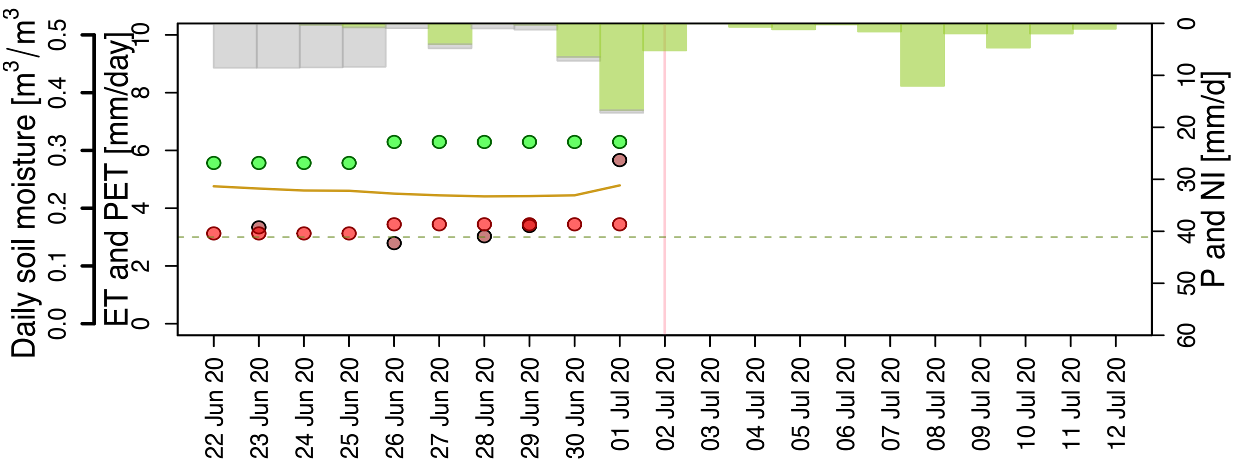

(a) Available observed variables for farm S2 on a give day such as 2020/07/02.

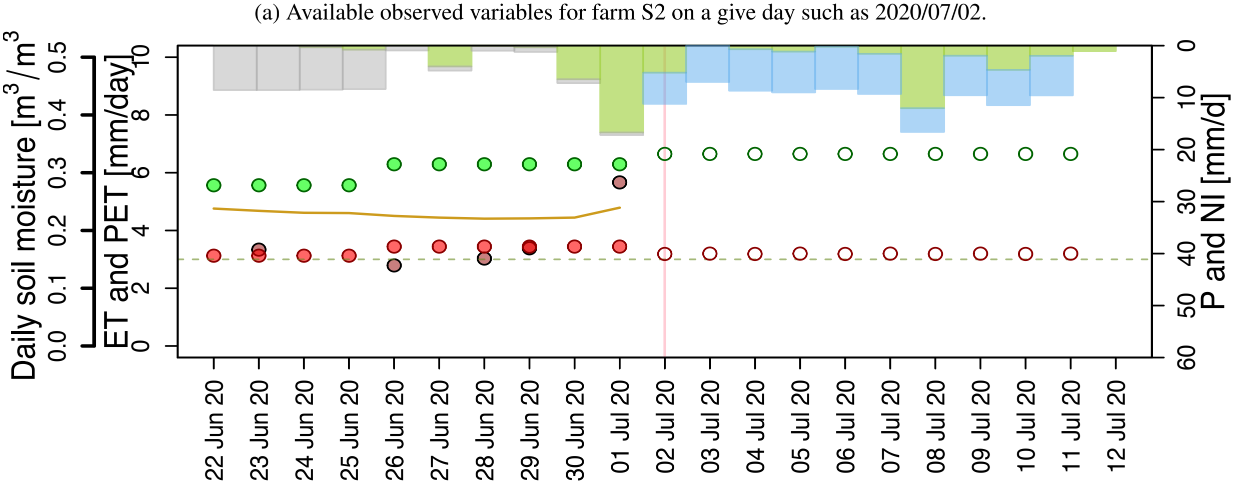

(b) Farm S2, after prediction using RF.

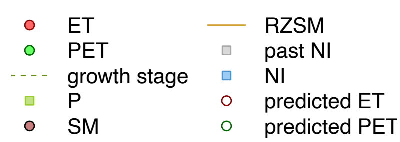

Figure 7. Farm S2 before and after prediction relative to the date 2020/07/02. Over the next 10 days the total predicted PET = 67 mm, total predicted ET = 32 mm, total P = 30 mm and NI = 71 mm.

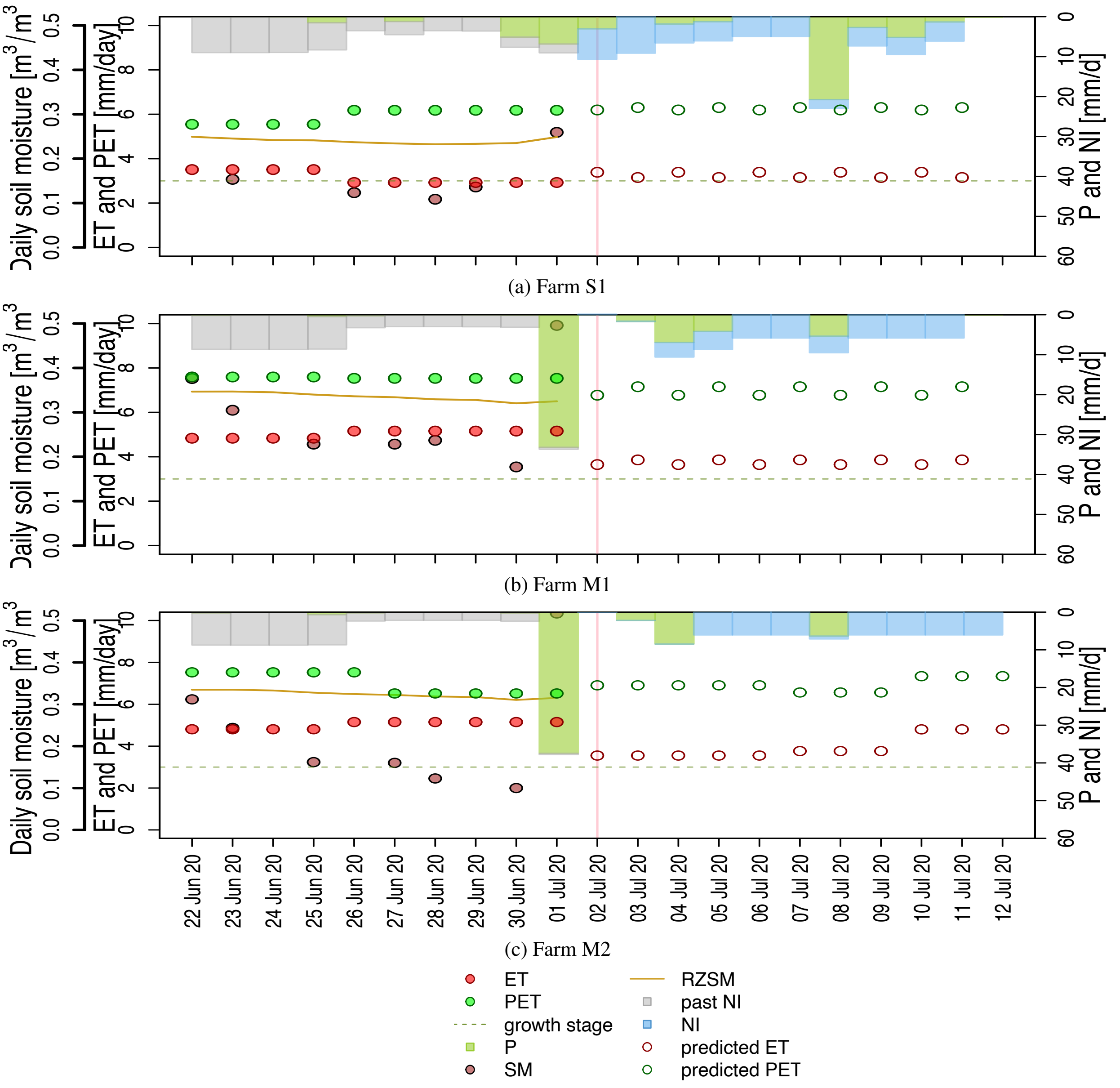

Figure 8. Predictions from farms S1, M1, and M2 for 2020/07/02. Total predicted values for the remaining 10 days are: Farm S1: PET = 62 mm, ET = 33 mm, P = 36 mm and NI = 52 mm. Farm M1: PET = 70 mm, ET = 38 mm, P = 18 mm and NI = 41 mm. Farm M2: PET = 76 mm, ET = 4 mm, P = 17 mm and NI = 43 mm. Growth stage is the phenological stage of the crop.

4.6 Tool Validation

For validation, we performed a spatial and temporal generalization test to understand FarmCan's ability to train and predict all days of crop planting in 2020 and for all of the 4 study farms using R^2, RMSE, and KGE parametric tests. The ability of the FarmCan model to generalize the spatial regions (farms) was assessed by comparing these values.

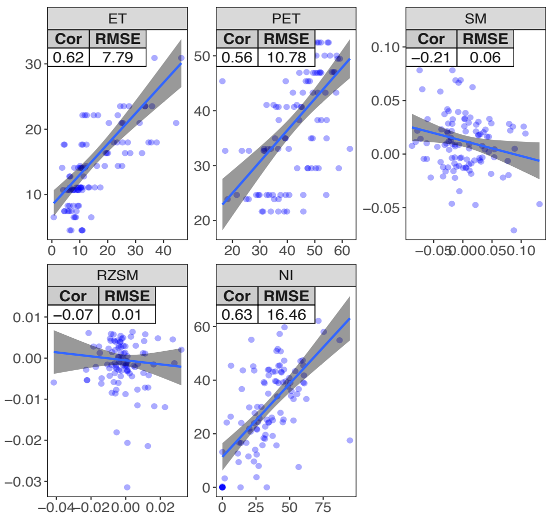

(a) Farm S1

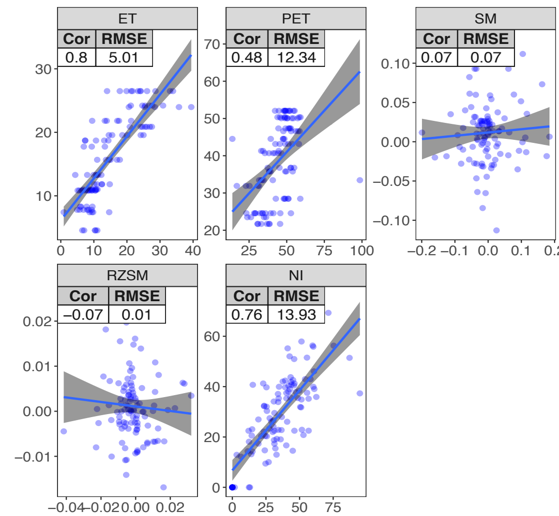

(b) Farm S2

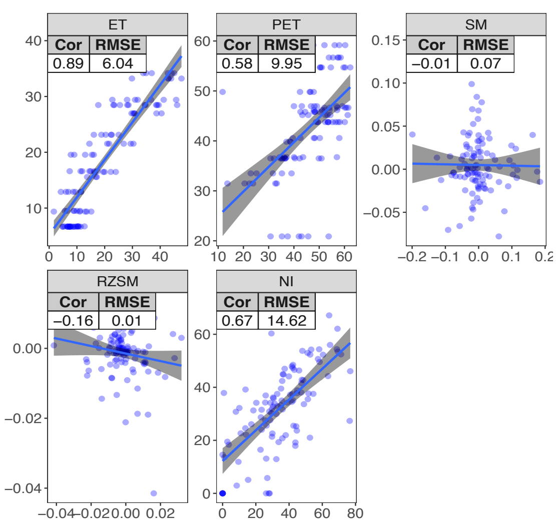

(c) Farm M1

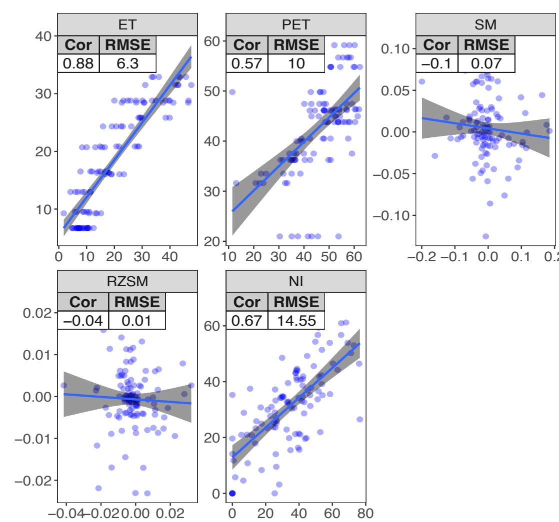

(d) Farm M2

Figure 9. 8-day correlation and RMSE plots for agricultural periods of Farms S1, S2, M1, and M2 [2015-2020]. Horizontal axes show observed values. Vertical axes are predicted. Note that the predicted NI is indirectly calculated from all the predicted variables. The crop is barely for the duration of 150 days of planting each year. Grey shades aid the eye in seeing linear patterns using a “lm” smoothing function.

Figure 10 shows the R^2 and RMSE values between the testing and predicted values of NI in all the study farms during the agricultural periods from 2015 to 2020. FarmCan showed the highest R^2 between observed and predicted values of 8-day ET, 8-day PET, and 8-day NI, and the lowest RMSE for ΔRZSM and ΔSM values. The high R^2 and high RMSE for 8-day NI values suggest that the amount of NI might be under-predicted in FarmCan, although the model captured the temporal patterns of water deficiency well. Table 5 shows the KGE values of 8-day ET, 8-day PET, and 8-day NI for the four study farms.

Table 5. KGE values of different covariates for different farms.

Farm	ET	PET	NI
S1	0.70	0.52	0.59
S2	0.72	0.46	0.67
M1	0.72	0.54	0.63
M2	0.70	0.54	0.60

KGE test is the goodness of fit. Generally, values higher than 0.41 are considered reasonable and satisfactory model performance, but there has not been a direct reason to choose this benchmark across all models (Knoben et al., 2019). We consider $0.5 \leq$ KGE satisfactory in this study. The model's goodness-of-fit is reasonable for ET, PET, and NI. The KGE values of ΔSM and ΔRZSM (not shown) have been zero or very close to zero. Here, KGE's negative values do not necessarily indicate a model that performed worse than the mean benchmark. The reason is that the range of Δ values of SM and RZSM was relatively small (approx. [-0.87,0.03] m^3/m^3), making the values very sensitive to the statistical tests. For the same reasons, it was expected that ΔSM and ΔRZSM did not show a good correlation, although they showed the lowest RMSE values (Figure 10). Given the satisfactory performance in final NI calculations, ΔSM and ΔRZSM predictions did not negatively affect the model and NI.

Generally, there is inherent uncertainty in FarmCan forecasts since we cannot know the actual value of the water deficiency and other controlling factors that maximize the crop yield. However, despite the unknowns, FarmCan showed an effective prediction capability to improve our understanding of NI and some of its main controlling factors in the CPE.

With the FarmCan model, we can select any number of CPE farms from airborne imagery, retrieve their spaceborne data, and forecast each farm's crop-specific water supply and demand to calculate water deficit.

This tool is versatile enough to allow access to any farm's critical hydroclimatic information for best water-related decision-making without stepping into the farm or setting up expensive monitoring equipment.

5 Conclusions

In this study, we develop the FarmCan model to bridge the gap between scientific modeling and practical, easy-to-understand water management decisions. FarmCan is a parsimonious supply-demand crop water monitor and forecasting mechanism. We demonstrated the potential of managing sustainable productivity of the land by timing and tuning of water available to the crops. The algorithm used NASA's NRT remote sensing data representing both atmospheric and soil properties coupled with the farm-specific information, water balance, and ML information to generate crop NI up to 14 days in advance, as well as the historical graphs for the farm.

For daily predictions, we used RF using 3-week data from one week prior, the current week, and one week over, and the data from the same days in the past years. This functionality allowed the FarmCan algorithm to take care of the seasonal variability automatically. In the next step, FarmCan will use the MSWX product, which enables this tool to function in real-time and as a prediction tool.

We showed ET and SM's relative importance in understanding NI's predictive value in the CPE. Compared to the daily data, we found that 8-day composite variables are stronger calculators for predicting NI as the 8-day tempers the inherent lags associated with P, soil, and atmospheric demand interactions. In addition, the phenological stage of the crop had a determinant factor in using ΔSM or ΔRZSM in the model.

In all four study farms, RF was effectively applied to predict the variables. The correlation between observed and predicted 8-day PET showed an average of 54%, and the 8-day NI forecast showed an average correlation of 68%. On the other hand, the correlation values between observed and predicted ΔSM or ΔRZSM were almost zero. Given the small range of variability in Δ values, the correlation numbers can not be indicators of the lack of contribution of soil moisture in the model.

The KGE values of RF predictions for the 8-day ET and 8-day PET showed an average of 0.71 and 0.50, respectively. Overall, FarmCan could forecast 8-day NI for the four farms with an average KGE of 0.62.

We saw a minimal impact on fluxes between ET and SM in the CPE during the agricultural year. We speculate that is due to the climate of the CPE. During the growing season, the condition in CPE is either too wet, which makes the total energy for ET independent of SM, or too dry, which makes ET show little impact on fluxes because it is little or no moisture available. However, more studies are required to understand the feedback between ET and SM in other environments. For example, in transitional environments, we expect to see that the total energy of ET is more dependent on SM.

We quantitatively showed that in the rainfed farms in the CPE, optimum crop production in the dry season should only be possible with an extra water supply. Crop production in some years may be possible but unreliable. Climate change will further affect this situation, and farmers are encouraged to move toward water management and adaptation strategies. Future studies can focus on such water shortages' social and economic implications (crop loss, reduced yield, water costs).

Future developments will focus on the role of the water retention capacity of the soil and crop type as two critical factors potentially affecting NI measurements. Plants in sandy soils, for example, may undergo water stress quicker when water is deficient. In contrast, plants in deep clay and fine texture may have ample time to adjust to low moisture conditions and remain unaffected by water deficiencies.

Future developments will also address how farmers can access FarmCan data, how supplementary irrigation versus rain-only farming can help farm cost/benefit management, and how the NI predictions and management advisory aid in better on-farm water management and crop yield. Coupling fertilization timing and the amount is another direction that can benefit farmers. Receiving feedback data from the farm managers will allow for yield and cost-benefit analyses.

Despite the inherent uncertainty in FarmCan forecasts, FarmCan is a step toward providing knowledge that can assist farm managers in making better decisions about excess water needs, drainage requirements, timing, and fertilizer consumption.

Author contributions. Sara Sadri: Conceptualization, Methodology, Software, Formal analysis, Writing original and final draft; Ming Pan: Resources, Methodology, Editing, Consulting; Aaron Berg: Editing, Consulting; Hylke Beck: Resources, Editing; James S. Famiglietti: Resources, Consulting, Editing; and Eric F. Wood: Conceptualization, Consulting

Abbreviations

CLSM Catchment land Surface Model

ET Evapotranspiration

FAO Food and Agricultural Organization

GEOS Goddard Earth Observation System

LAI Leaf Area Index

ML Machine Learning

MSWEP Multi-Source Weighted-Ensemble Precipitation

MODIS Moderate Resolution Imaging Spectroradiometer

NI Needed Irrigation

NRT Near-Real-Time

PET Potential Evapotranspiration

P Precipitation

RF Random Forest

RZSM Root Zone Soil Moisture

SMAP Soil Moisture Active Passive

SM (Surface) Soil Moisture

WUE Water Use Efficiency

Competing interests. The authors declare that they have no known competing financial interests or personal relationships that could have appeared to influence the work reported in this paper.

References

Al Bitar, A., Mialon, A., Kerr, Y. H., Cabot, F., Richaume, P., Jacquette, E., Quesney, A., Mahmoodi, A., Tarot, S., Parrens, M., Al-Yaari, A., Pellarin, T., Rodriguez-Fernandez, N., and Wigneron, J.-P.: The global SMOS Level 3 daily soil moisture and brightness temperature maps, Earth System Science Data, 9, 293–315, 2017.

Allen, R., Pereira, L., Raes, D., and Smith, M.: HYDRUS-2D simulations of water and potassium movement in drip irrigated tropical soil container cultivated with sugarcane, FAO Irrigation and Drainage, 56, food and Agriculture Organization of the United Nations, Rome, 1998a.

Allen, R., Tasumi, M., and Trezza, R.: Satellite-based energy balance for mapping evapotranspiration with internalized calibration (METRIC)-Model, Journal of Irrigation and Drainage Engineering, 133, 380–394, 2007.

Allen, R. G., Pereira, L. S., Raes, D., and Smith, M.: Crop evapotranspiration - Guidelines for computing crop water requirements - FAO Irrigation and drainage paper 56, Online, Rome, Italy, http://www.fao.org/3/X0490E/X0490E00.htm, 1998b.

Andarzian, B., Bannayan, M., Steduto, P., Mazraeh, H., Barati, M., Barati, M., and Rahnama, A.: Validation and testing of the AquaCrop model under full and deficit irrigated wheat production in Iran, Agricultural Water Management, 100, 1–8, https://doi.org/https://doi.org/10.1016/j.agwat.2011.08.023, 2011.

Ash, G., C, C. S., and Raddatz, R.: Moisture risk assessment for spring wheat on the eastern Prairies: a water use simulation model, Climatol Bull, 26, 65–78, 1992.

Beck, H., Wood, E., Pan, M., Fisher, C., van Dijk, D. M. A., and Adler, T. M. R.: MSWEP V2 global 3-hourly 0.1 precipitation: methodology and quantitative assessment, Bulletin of the American Meteorological Society, 100, 473–500, 2019.

Beck, H. E., van Dijk, A. I. J. M., Larraondo, P. R., McVicar, T. R., Pan, M., Dutra, E., and Miralles, D. G.: MSWX: Global 3-hourly 0.1 bias-corrected meteorological data including near-real-time updates and forecasted ensembles, Bulletin of the American Meteorological Society, 103, E701–E732, 2022.

Bhuiyan, H. A., McNairn, H., Powers, J., Friesen, M., Pacheco, A., Jackson, T. J., Cosh, M. H., Colliander, A., Berg, A., Rowlandson, T., Bullock, P., and Magagi, R.: Assessing SMAP Soil Moisture Scaling and Retrieval in the Carman (Canada) Study Site, Vadose Zone Journal, 17, 1–14, 2018.

Bonsal, B. R., Zhang, X., and Hogg, W. D.: Canadian Prairie growing season precipitationvariability and associated atmospheric circulation, CLIMATE RESEARCH, 11, 191–208, 1999.

Breiman, L.: Random forests, Machine Learning, 45, 5–32, 2001.

Brouwer, C. and Heibloem, M.: Irrigation Water Management: Irrigation Water Needs, Training manual no. 3, Food and Agriculture Organization of the United Nations, Via delle Terme di Caracalla, 00100 Rome, Italy, http://www.fao.org/3/s2022e/s2022e00.htm#Contents, 1986.

Brust, C., Kimball, J. S., Maneta, M. P., Jencso1, K., and Reichle, R. H.: DroughtCast: A Machine Learning Forecast of the United States Drought Monitor, Frontiers in Big Data, 2021.

Chalmers, D., Mitchell, P., and Heek, L. V.: Control of peach tree growth and productivity by regulated water supply, tree density, and summer pruning [Trickle irrigation], J. Am. Soc. Hortic. Sci., 106, 307–312, 1981.

Cherneski, P.: The Impacts and Costs of Drought to the Canadian Agriculture Sector, https://www.drought.gov/nadm/sites/drought.gov.nadm/files/activities/2018Workshop/8_3_CHERNESKI-Agricultural_Drought_Impacts_Canada.pdf, saskatchewan, Canada, 2018.

Clewley, D., Whitecomb, J., Akbar, R., Silva, A., Berg, A., Adams, J., Caldwell, T., and coauthors: A Method for Upscaling In Situ Soil Moisture Measurements to Satellite Footprint Scale Using Random Forests, IEEE Journal of Selected Topics in Applied Earth Observations and Remote Sensing, 10, 2663–2673, 2017.

ECCC: Annual Crop Inventory, https://open.canada.ca/data/en/dataset/ba2645d5-4458-414d-b196-6303ac06c1c9, 2013.

Entekhabi, D., Das, N., Njoku, E., Yueh, S., Johnson, J., and Shi, J.: Algorithm Theoretical Basis Document L2 & L3 Radar/Radiometer Soil Moisture (Active/Passive) Data Products, Document, JPL, 2014.

Famiglietti, J. S. and Wood, E. F.: Multiscale modeling of spatially variable water and energy balance process, Water Resour. Res., 30, 3061–3078, 1994.

FAO: How to Feed the World in 2050, http://www.fao.org/fileadmin/templates/wsfs/docs/expert_paper/How_to_Feed_the_World_in_2050.pdf, 2009.

Fisher, J., Melton, F., Middleton, E., Hain, C., Anderson, M., Allen, R., McCabe, M. F., Hook, S., Baldocchi, D., Townsend, P. A., Kilic, A., Tu, K., Miralles, D. D., Perret, J., Lagouarde, J., Waliser, D., Purdy, A. J., French, A., Schimel, D., Famiglietti, J. S., Stephens, G., and Wood, E. F.: The future of evapotranspiration: Global requirements for ecosystem functioning, carbon and climate feedbacks, agricultural management, and water resources, Water Resources Research, 53, 2618–2626, 2017.

Franz, T., Heeren, D., Pokal, S., Gholizadeh, H., Rudnick, D., Jin, Z., Tenorio, F., Zhou, Y., Gibson, J., Gates, J., McCabe, M., Guan, K., Ziliani, M., Pan, M., and Wardlow, B.: The role of topography, soil, and remotely sensed vegetation condition towards predicting crop yield, Field Crops Research, 252, 2020.

Geerts, S. and Raes, D.: Deficit irrigation as an on-farm strategy to maximize crop water productivity in dry areas, Agricultural Water Management, 96, 1275–1284, 2009.

Hadwen, T. and Schaan, G.: The 2017 Drought in the Canadian Prairies, Report, Agriculture Agrifood Canada, https://www.preventionweb.net/files/78461_cs4.gar2017canadianprairiesdroughtc.pdf, (Last accessed September 2021), 2017.

Han, M., Zhang, H., DeJonge, K. C., Comas, L. H., and Gleason, S.: Comparison of three crop water stress index models with sap flow measurements in maize, Agricultural Water Management, 203, 366–375, 2018.

I.Seneviratne, S., Corti, T., L.Davin, E., Hirschi, M., B.Jaeger, E., Lehner, I., Orlowsky, B., and J.Teuling, A.: Investigating soil moisture-climate interactions in a changing climate: A review, Earth-Science Reviews, 99, 125–161, 2010.

Jia, Y., Shen, S., Niu, C., Qiu, Y., Wang, H., and Liu, Y.: Coupling crop growth and hydrologic models to predict crop yield with spatial analysis technologies, J. Appl. Remote Sens., 5, 1–20, 2011.

Kirda, C.: Deficit Irrigation Practices - Deficit irrigation scheduling based on plant growth stages showing water stress tolerance, Report 22, Cukuroya University, Rome, Italy, https://www.fao.org/3/y3655e/y3655e00.htm#TopOfPage, 2000.

Knoben, W., J.E.Freer, and Woods, R.: Technical note: Inherent benchmark or not? Comparing NashSutcliffe and Kling-Gupta efficiency scores, HESS Discussions, 2019.

Koster, R., Guo, Z., Yang, R., Dirmeyer, P., Mitchell, K., and Pum, M.: On the nature of soil moisture in land surface models, J. Clim., 22, 4322–4335, 2009.

L. Chen, L. and Dirmeyer, P.: Impacts of land-use/land-cover change on afternoon precipitation over North America, J. Climate, 30, 2121–2140, 2017.

Levidowa, L., Zaccariab, D., Maiac, R., Vivasc, E., Todorovicd, M., and Scardigno, A.: Improving water-efficient irrigation: Prospects and difficulties of innovative practices, Agricultural Water Management, 146, 84–94, 2014.

Liu, Q., Reichle, R. H., Bindlish, R., Cosh, M. H., Crow, W. T., de Jeu, R., Lannoy, G. J. M. D., Huffman, G. J., and Jackson, T. J.: The contributions of precipitation and soil moisture observations to the skill of soil moisture estimates in a land data assimilation system, Journal of Hydrometeorology, 12, 750–765, 2011.

Loggenberg, K., Strever, A., Greyling, B., and Poona, N.: Modelling water stress in a Shiraz Vineyard using hyperspectral imaging and machine learning, Remote Sensing, 10, 202, 2018.

Martens, B. and Coauthors: GLEAM v3: Satellitebased land evaporation and root-zone soil moisture, Geosci. Model Dev.,, 10, 1903–1925, 2017.

Maybank, J., Bonsal, B., Jones, K., Lawford, R., O'Brien, E., Ripley, E., and Wheaton, E.: Drought as a natural disaster, Atmosphere-Ocean, 33, 195–222, 1995.

McGinn, S. and Shepherd, A.: Impact of climate change scenarios on the agroclimate of the Canadian prairies, Canadian Journal of Soil Science, 83, 623–630, 2003.

Papagiannopoulou, C., D.G. Miralles, W. D., Verhoest, N., Depoorter, M., and Waegeman, W.: Vegetation anomalies caused by antecedent precipitation in most of the world, Environ. Res. Lett, 12, 074 016, 2017.

Pendergrass, A. G., Meehl, G. A., Pulwarty, R., Hobbins, M., Hoell, A., AghaKouchak, A., Bonfils, C. J. W., Gallant, A. J. E., Hoerling, M., Hoffmann, D., Kaatz, L., Lehner, F., Llewellyn, D., Mote, P., Neale, R. B., Overpeck, J. T., Sheffield, A., Stahl, K., Svoboda, M., Wheeler, M. C., Wood, A. W., and Woodhouse, C. A.: Flash droughts present a new challenge for subseasonal-to-seasonal prediction, Nature Climate Change, 10, 191–199, https://doi.org/https://doi.org/10.1038/s41558-020-0709-0, 2020.

Poblete, T., Ortega-Farias, S., and Bardeen, M. M. M.: Artificial neural network to predict vine water status spatial variability using multispectral information obtained from an unmanned aerial vehicle (UAV), Sensors, 17, 2488, 2017.

Poccas, I., Gonccalves, J., Costa, P., Gonccalves, I., Pereira, L., and Cunha, M.: Hyperspectral-based predictive modelling of grapevine water status in the portuguese douro wine region, International Journal of Applied Earth Observation and Geoinformation, 58, 177–190, 2017.

Pomeroy, J., Nicholaichuk, W., Cray, D., McConkey, B., Cranger, R., and Landine, P.: SNOW MANAGEMENTAND MELTWATER ENHANCEMENT FINAL REPORT, Tech Report CS-90021, Nationl Hydrology Research Institute, Environment Canada, 11 innovation Bivd., Sasiatoon, Saskatchewan S7N 3H5, http://citeseerx.ist.psu.edu/viewdoc/download?doi=10.1.1.725.7817&rep=rep1&type=pdf, (Last accessed September 2021), 1990.

Quiring, S.: Growing-season moisture variability in the eastern USA during the last 800 years, Clim Res, 27, 9–17, 2004.

Rapaport, T., Hochberg, U., Shoshany, M., Karnieli, A., and Rachmilevitch, S.: Combining leaf physiology, hyperspectral imaging and partial least squares-regression ($PLS-R$) for grapevine water status assessment, ISPRS Journal of Photogrammetry and Remote Sensing, 109, 88–97, 2015.

Reichle, R., Lucchesi, R., Ardizzone, J. V., Kim, G., Smith, E. B., and Weiss, B. H.: Soil Moisture Active Passive (SMAP) Mission Level 4 Surface and Root Zone Soil Moisture (L4SM) Product Specification Document, Tech. Rep. 10 (Version 1.4), NASA Goddard Space Flight Center, Greenbelt, MD, 2015.

Reichle, R. H.: Assessment of the SMAP Level-4 Surface and Root-Zone Soil Moisture Product Using In Situ Measurements, Journal of Hydrometeorology, 18, 2621–2645, 2017.

Reichle, R. H., Koster, R. D., Lannoy, G. J. M. D., Forman, B. A., Liu, Q., Mahanama, S. P. P., and Toure, A.: Assessment and enhancement of MERRA land surface hydrology estimates, Journal of Climate, 24, 6322–6338, 2011.

Reichle, R. H., Liu, Q., Koster, R. D., Crow, W. T., Lannoy, G. J. M. D., Kimball, J. S., Ardizzone, J. V., Bosch, D., Colliander, A., Cosh, M., Kolassa, J., Mahanama, S. P., Prueger, J., Starks, P., and Walker, J. P.: Version 4 of the SMAP Level-4 Soil Moisture Algorithm and Data Product, Journal of Advances in Modeling Earth Systems, 11, 3106–3130, 2019.

Rienecker, M., Suarez, M., Todling, R., Bacmeister, J., Takacs, L., Liu, H.-C., Gu, W., Sienkiewicz, M., Koster, R., Gelaro, R., Stajner, I., and Nielsen, J.: The GEOS-5 Data Assimilation System - Documentation of Versions 5.0.1, 5.1.0, and 5.2.0., NASA Technical Report Series on Global Modeling and Data Assimilation NASA/TM-2008-104606, NASA, vol. 28, 101 pp., 2008.

Romero, M., Luo, Y., Su, B., and Fentes, S.: Vineyard water status estimation using multispectral imagery from an UAV platform and machine learning algorithms for irrigation scheduling management, Computers and Electronics in Agriculture, 147, 109–117, 2018.

Running, S.: MOD16A2 v006, LP DAAC, https://lpdaac.usgs.gov/products/mod16a2v006/, 2001.

Running, S. W., Mu, Q., Zhao, M., and Moreno, A.: MODIS Global Terrestrial Evapotranspiration (ET) Product (MOD16A2/A3 and Year-end Gap-filled MOD16A2GF/A3GF) NASA Earth Observing System MODIS Land Algorithm, Tech. rep., NASA, (Last access, 2019.

Sadri, S., Wood, E. F., and Pan, M.: Developing a drought-monitoring index for the contiguous US using SMAP, Hydrol. Earth Syst. Sci., 22, 6611–6626, 2018.

Sadri, S., Pan, M., Wada, Y., Vergopolana, N., Sheffield, J., Famigliettie, J. S., Kerr, Y., and Wood, E.: A global near-real-time soil moisture index monitor for food security using integrated SMOS and SMAP, Remote Sensing of Environment, 246, 1–22, 2020.

Saini, R. and Ghosh, S.: Crop classification on single date sentinel-2 imagery using random forest and support vector machine, International Archives of the Photogrammetry, Remote Sensing and Spatial Information Sciences, XLII, 683–688, 2018.

Saskatchewan Government: Irrigation Development Process, https://www.saskatchewan.ca/business/agriculture-natural-resources-and-industry/agribusiness-farmers-and-ranchers/crops-and-irrigation/irrigation/irrigation-development-process, 2022.

ScienceDaily: Scientists propose improvements to precision crop irrigation, University of Illinois, College of Agricultural, Consumer and Environmental Sciences, www.sciencedaily.com/releases/2021/04/210429112359.htm, (accessed September 2, 2021), 2021.

Shuval, H. and Dweik, H.: Water Resources in the Middle East, Israel-Palestinian Water Issues- From Conflict to Cooperation, vol. 2, Springer, Jerusalem, Israel, https://www.google.com/books/edition/Water_Resources_in_the_Middle_East/SW67ZNZM-lIC?hl=en&gbpv=1&printsec=frontcover, p. 80, 136, 2007.

Smilovic, M., Gleeson, T., and Adamowski, J.: Crop kites: Determining crop-water production functions using crop coefficients and sensitivity indices, Advances in Water Resources, 97, 193–204, 2016.

Smilovic, M., Gleeson, T., Adamowski, J., and Langhorn, C.: More food with less water-Optimizing agricultural water use, Advances in Water Resources, 123, 256–261, 2019.

Sonth, M. V., Ambesange, S., Sreekanth, D., and Tulluri, S.: Optimization of Random Forest Algorithm with Ensemble and Hyper Parameter Tuning Techniques for Multiple Heart Diseases, Solid State Technology, 63, 2020.

Taghvaeian, S., Andales, A. A., Allen, L. N., Kisekka, I., O'Shaughnessy, S. A., Porter, D. O., Sui, R., Irmak, S., Fulton, A., and Aguilar, J.: Irrigation Scheduling for Agriculture in the United States: The Progress Made and the Path Forward, Transactions of the ASABE, 63, 1603–1618, 2020.

Tetlock, E., Toth, B., Berg, A., Rowlandson, T., and Ambadan, J.: An 11-year (2007-2017) soil moisture and precipitation dataset from the Kenaston Network in the Brightwater Creek basin, Saskatchewan, Canada, Earth System Science Data, 11, 787–796, 2019.

Th.F.Stocker, D. Qin, G.-K. P., Tignor, M., S.K.Allen, Boschung, J., Nauels, A., Xia, Y., Bex, V., and Midgley, P.: Climate Change 2013– The Physical Science Basis: Working Group I Contribution to the Fifth Assessment Report of the Intergovernmental Panel on Climate Change, Cambridge University Press, Cambridge, United Kingdom and New York, NY, USA, 2013.

UN/ISDR: Drought Risk Reduction Framework and Practices: Contributing to the Implementation of the Hyogo Framework for Action. United Nations Secretariat of the International Strategy for Disaster Reduction (UN/ISDR), Tech. Rep. 98+vi pp, United Nations Secretariat of the International Strategy for Disaster Reduction (UN/ISDR), Geneva, Switzerland, 2007.

USDA-NASS: Irrigation and Water Management Survey, https://www.nass.usda.gov/Surveys/Guide_to_NASS_Surveys/Farm_and_Ranch_Irrigation/index.php, washington, DC, 2021.

Vergopolan, N., Xiong, S., Estes, L., Wanders, N., Chaney, N. W., Wood, E. F., Konar, M., Caylor, K., Beck, H. E., Gatti, N., Evans, T., and Sheffield, J.: Field-scale soil moisture bridges the spatial-scale gap between drought monitoring and agricultural yields, Hydrology and Earth System Sciences, 25, 1827–1847, https://doi.org/10.5194/hess-25-1827-2021, 2021.

Virnodkar, S., Pachghare, V., and V.C, . P. V. e. a.: Remote sensing and machine learning for crop water stress determination in various crops: a critical review, Precision Agric, 21, 1121–1155, 2020.

Wanders, N., Karssenberg, D., Roo, A., Jong, S. D., and Bierkens, M.: The suitability of remotely sensed soil moisture for improving operational flood forecasting, Hydrol. Earth Syst. Sci., 18, 2343–2357, 2014.

Wheaton, E., Wittrock, V., Kulshreshtha, S., Koshida, G., C, C. G., Chipanshi, A., and Bonsal, B.: Lessons Learned from the Canadian Drought Years of 2001 and 2002: Synthesis Report for Agriculture and Agri-Food Canada, Tech. Rep. [SRC publication no. 11602-46E03, Saskatoon: Saskatchewan Research Council, Saskatoon, 2005.

White, J., Berga, A. A., Champagneb, C., Zhangb, Y., Chipanshi, A., and Daneshfar, B.: Improving crop yield forecasts with satellite-based soil moisture estimates: An example for township level canola yield forecasts over the Canadian Prairies, Int J Appl Earth Obs Geoinformation, 89, 1–12, 2020.

Wittrock, V. and Ripley, E.: The predictability of autumn soil moisture levels on the Canadian Prairies, J Climatol, 19, 271–289, 1999.

Yang, Y., Donohue, R., and McVicar, T.: Global estimation of effective plants rooting depth: Implications for hydrological modeling, Water Resour. Res., 52, 8260–8276, 2016.

Yang, Y., Guan, K., Zhang, J., Peng, B., Pan, M., and Zhou, W.: Incorporating a plant water supply-demand farame-work into Noah-MP land surface model to simulate hydrological fluxes for agroecosystems, B046-0018, American Geophysical Union Fall Meeting, San Francisco, 2020.

Zohaib, M., Kim, H., and Choi, M.: Evaluating the patterns of spatiotemporal trends of root zone soil moisture in major climate regions in East Asia, J. Geophys. Res. Atmos., 122, 7705–7722, 2017.